

# Two dimensional laser induced fluorescence in the gas phase: a spectroscopic tool for studying molecular spectroscopy and dynamics

Jason R. Gascooke and Warren D. Lawrance<sup>a</sup>

School of Chemical and Physical Sciences, Flinders University, GPO Box 2100, Adelaide, SA 5001, Australia

Received 7 August 2017 / Received in final form 5 September 2017

Published online 14 November 2017 – © EDP Sciences, Società Italiana di Fisica, Springer-Verlag 2017

**Abstract.** Two dimensional laser induced fluorescence (2D-LIF) extends the usual laser induced fluorescence technique by adding a second dimension, the wavelength at which excited states emit, thereby significantly enhancing the information that can be extracted. It allows overlapping absorption features, whether they arise from within the same molecule or from different molecules in a mixture, to be associated with their appropriate “parent” state and/or molecule. While the first gas phase version of the technique was published a decade ago, the technique is in its infancy, having been exploited by only a few groups to date. However, its potential in gas phase spectroscopy and dynamics is significant. In this article we provide an overview of the technique and illustrate its potential with examples, with a focus on those utilising high resolution in the dispersed fluorescence dimension.

## 1 Introduction

Nuclear magnetic resonance (NMR) spectroscopy has been revolutionised by the introduction of two dimensional techniques, which have led to a significant increase in potential applications and usefulness [1–3]. It is thus natural to extend these ideas and techniques to other areas of spectroscopy and significant developments have been made in this regard, often involving non-linear optical techniques with short laser pulses, which also introduces the opportunity to extend to a third dimension of time [4–10]. Such techniques can be particularly useful in condensed phases where the sharp spectroscopic features that typically characterise gas phase samples are lost. However, the richness of features in gas phase spectra, particularly of polyatomic molecules, leads to its own complexity, with a structure that is often complicated and difficult to interpret. Consequently, there is also interest in developing new, multidimensional spectroscopic techniques to provide deeper insights when interrogating and assigning gas phase molecular spectra.

Methods based on coherent two dimensional (2D) spectroscopy designed for this purpose have been summarised by several authors [6–8]. Two-dimensional resonance enhanced multiphoton ionisation (2D-REMPI), where a time of flight mass spectrum is recorded at each laser wavelength, has been demonstrated to be a useful technique for identifying the species associated with new absorption features in gas phase samples [11]. For

molecules that fluoresce, an alternative to multiple laser techniques involves utilising the light emitted following optical excitation. Monitoring the emission spectrum as a function of excitation wavelength leads to the intensity being a function of the two optical wavelength dimensions (or, equivalently, frequency dimensions) of excitation and emission. The opportunity presented by observing spectral features in this way was recognised as long ago as 1961 by Weber, who proposed it as a means to determine the number of species in a solution mixture [12]. A device for measuring solution excitation and emission spectra simultaneously was reported some 15 years later [13]. Modern commercial fluorimeters often have the capability for providing such 2D scans for condensed phase samples and there have been recent developments in fast acquisition instrumentation specifically for this purpose [14].

In the case of gas phase studies, signal levels are generally much reduced compared with solution due to the low number densities required to ensure that emission occurs prior to collisions scrambling the initial excitation among a multitude of states. Dispersed fluorescence from single vibrational levels within the excited electronic state in the gas phase began in the early 1970s using Xe arc light sources [15–18] but within a decade the availability of tunable nanosecond dye lasers with frequency doubling had made so-called single vibronic level fluorescence a routine method for spectroscopic exploration of excited electronic states. High sensitivity photomultipliers were typically required for detection. It was not until 2006 that Reilly, Schmidt and Kable (RSK) showed that combining dispersed fluorescence and laser induced fluorescence (LIF)

<sup>a</sup> e-mail: [warren.lawrance@flinders.edu.au](mailto:warren.lawrance@flinders.edu.au)

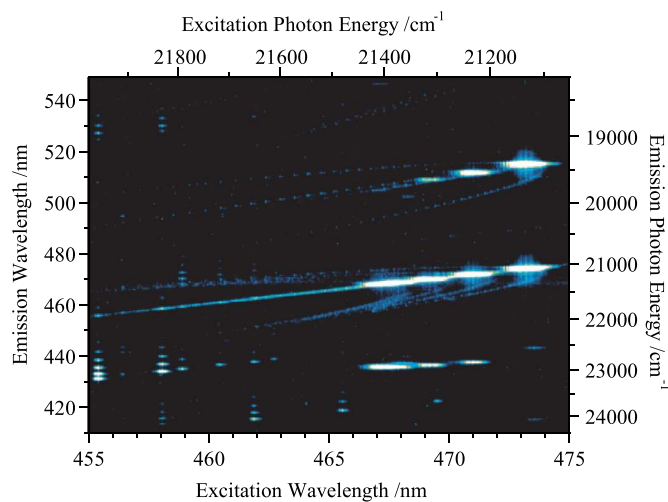


**Fig. 1.** The original 2D-LIF image from the paper by Reilly, Schmidt and Kable. (Adapted from Ref. [19].)

scanning into a single 2D spectral measurement provides a powerful method for identifying the various molecular species in a complex, gas phase chemical environment using a single laser [19]. By this time sensitive array detectors had been developed for monitoring the positions at which photons strike the detector. In the technique reported by RSK, the dispersed fluorescence spectrum is measured at each laser wavelength in a laser induced fluorescence (LIF) scan, resulting in a so-called two dimensional laser induced fluorescence (2D-LIF) spectral image, the two axes being the laser wavelength/frequency and fluorescence wavelength/frequency. (Note that the term 2D-LIF in this context refers to spectroscopy in two wavelength/frequency axes. This should not be confused with the technique of the same name used to obtain spatial information on chemical species in, for example, combustion, in which a cylindrically focused laser creates a “two dimensional excitation sheet”, with spatial detection of the resulting fluorescence [20].) In RSK’s experiment the fluorescence was dispersed using a spectrometer with a charge coupled device (CCD) array detector, allowing a large region of the fluorescence spectrum to be captured at each laser position, albeit at limited resolution. A plot of the fluorescence intensity as a function of the excitation and emission wavelengths enabled the emitting species to be identified, where the spectrum was known, and bands from new species to be revealed. This first gas phase 2D-LIF image is reproduced in Figure 1.

Over the past few years our group has developed the 2D-LIF technique in an alternative direction. We have developed the method as a spectroscopic tool for probing the rotational and vibrational features accompanying electronic transitions in polyatomic molecules, with a focus on achieving high resolution (ca.  $0.5\text{ cm}^{-1}$  or less) in the fluorescence dimension so that it is comparable with that of the excitation step when using a conventional commercial pulsed dye laser. This results in 2D rotational contours that are near-equally resolved in the excitation and emission dimensions, leading to easily recognisable shapes that allow multiple features to be extracted even when there is

significant overlap. The technique has been applied to a number of different spectroscopic “problems” to illustrate its power [21–28].

Although it is a decade since RSK published their first 2D-LIF gas phase work, 2D-LIF currently remains a niche technique. In this article we provide an overview of the 2D-LIF technique and show its usefulness and power through a number of examples. We hope that this will stimulate a wider uptake of the method.

## 2 The 2D-LIF technique

The 2D-LIF technique involves measuring the dispersed fluorescence spectrum, or a segment of it, at each laser wavelength as it is scanned step-wise over the desired absorption spectral region. In principle, by matching the detector size and spectrometer dispersion the entire dispersed fluorescence spectrum can be captured at each laser wavelength. However, in practice, the size of readily available detectors can limit the region monitored to a subset of the full spectrum. This is particularly the case when high fluorescence resolution is sought: in such cases a high dispersion spectrometer is required, which leads to the fluorescence spectrum being spread over a wide region at the spectrometer exit. There is thus a compromise to be made between spectral resolution and how much of the spectrum can be captured simultaneously. This can be illustrated by comparing the system used by RSK [19] with that used in our work [21]. 2D-LIF spectral images from the two laboratories are shown in Figures 1 and 2, respectively, and we draw the reader’s attention to the different scales on the fluorescence axes in the two images. RSK did not require high resolution, but required a large spectral region to be monitored in order to differentiate emitting species. Their experiment used a small spectrometer that was set to detect a spectral region  $\sim 6200\text{ cm}^{-1}$  wide centred at ca. 480 nm. Although the spectral resolution was not specified, the peaks in extracted spectra indicate a linewidth  $\sim 30\text{ cm}^{-1}$ . In contrast, our high resolution experiments utilise a large spectrometer with a dispersion  $\sim 5\text{ cm}^{-1}/\text{mm}$  at the exit plane at 250 nm. With our 25 mm diameter image intensifier detector, this gives a practical width of ca.  $90\text{ cm}^{-1}$  when the entrance slit height, and thus vertical signal dimension, is allowed for. The reduction in spectral range is the compromise required for the increase in resolution: we routinely operate the spectrometer at a resolution of  $0.5\text{ cm}^{-1}$  in the 250 nm region, which is comparable with typical commercial nanosecond pulsed laser linewidths. A doubling of the diameter of the image intensifier would be straightforward, with commercial devices available, but even so this only doubles the spectral region monitored.

The experiment in our laboratory runs as follows. A pulsed dye laser (duration  $\sim 5\text{ ns}$ ) is wavelength scanned in discrete steps across the region of interest. At each wavelength it is “parked” for a pre-set number of shots while a dispersed fluorescence spectrum is obtained, and it is then stepped to the next wavelength where the next dispersed fluorescence spectrum is measured, with the process continuing until the scan region has been covered. An image

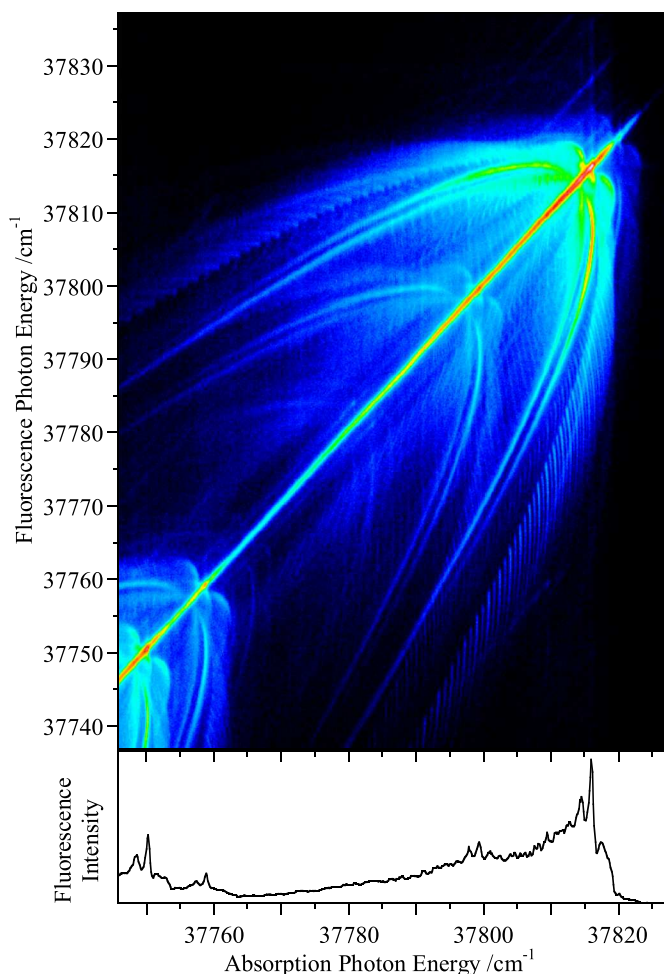


**Fig. 2.** An example of a 2D-LIF image with high resolution in the fluorescence dimension. The image shows the  $0_0^0$  transition of a room temperature sample of fluorobenzene, which is responsible for the main features of the image. The spectrum shown below the image is the laser induced fluorescence (LIF) spectrum generated by projecting the 2D-LIF image onto the laser (absorption) axis. (Adapted from Ref. [21].)

intensifier with single photon detection sensitivity is used to capture a region of the dispersed fluorescence spectrum. The image intensifier is gated to detect fluorescence in a time window coincident with the laser pulse. The gate width is variable and typically set to several times the fluorescence lifetime. The image intensifier produces bright spots on a phosphor screen corresponding to the positions where photons strike its front face. The phosphor screen is imaged onto a CCD camera using a conventional camera lens. The CCD output is read each laser shot by a computer and analysed to identify and record the centre of each photon spot observed. This information is used to build up a histogram of photon count at each camera pixel position. When scans involve a high number of laser shots at each wavelength, the 2D-LIF image is recorded multiple times with a low number of laser shots per laser wavelength and the resulting images summed to produce the final image. This minimises the effects of

slowly fluctuating laser power that can be an issue during a single long scan. The spectrometer is calibrated before each scan for the region being monitored using scattered light from a dye laser whose wavelength is calibrated using a wavemeter.

An example of a 2D-LIF image with high resolution in the fluorescence dimension is shown in Figure 2 [21]. The image shows the  $0_0^0$  transition of fluorobenzene, which is responsible for the main features of the image. Where the focus is on the excitation spectrum as in this example, the 2D-LIF images are presented with the laser wavenumber along the  $x$ -axis and the fluorescence wavenumber along the  $y$ -axis. Features are labelled by their  $(x, y)$  value, i.e. the (absorption, emission) wavenumber values. The energies in both the excited ( $S_1$ ) and ground electronic ( $S_0$ ) states for the features observed can be determined from their positions in the 2D-LIF spectral image. The change in laser wavelength during a scan leads to a change in its position as measured by the spectrometer and, because in our instrument the laser scan step size and the wavelength between adjacent fluorescence pixels are very similar, the laser traces a “diagonal” line across the 2D-LIF image (bottom left to top right). The symmetric “wings” about the image diagonal that sweep back to lower energy are associated with the rotational structure arising from the rotational transitions occurring during absorption and fluorescence. Shifted along the image diagonal to lower energy are several sequence bands, each displaying the same rotational pattern as  $0_0^0$ . The symmetry about the diagonal arises because a feature on the image at  $(m, n)$  corresponds to laser excitation at  $m \text{ cm}^{-1}$  and fluorescence at  $n \text{ cm}^{-1}$  and, since both transitions are allowed, there is a corresponding point  $(n, m)$  arising from laser excitation at  $n \text{ cm}^{-1}$  and fluorescence at  $m \text{ cm}^{-1}$ . This results in reflection symmetry about the image diagonal. The intensities of the two related transitions differ, primarily because of the different initial state Boltzmann populations. The 2D-LIF spectral image is easily integrated along the dispersed fluorescence axis to give the more familiar LIF spectrum, shown in the lower panel of Figure 2 for comparison.

Features originating in different  $S_1$  states but terminating in the same  $S_0$  state lie along lines that run parallel to the image “diagonal” discussed above. For data analysis it can be preferable to “skew” the images to convert the “diagonal” into a horizontal line and all fluorescence transitions terminating in the same state now lie on a horizontal line. In our applications this is done during the analysis using software [23,24]. An example of a skewed image is shown in Figure 3. However, particularly where scans over a large wavelength region are conducted, fluorescence features can shift off the detector and it is preferable to step the spectrometer synchronously with the laser such that the laser is maintained at a constant position on the detector during the scan. Steimle and co-workers have pioneered this approach [29].

An important characteristic of a high resolution 2D-LIF image is the shape of the spectral features. In conventional (1D) spectroscopy, rotational contours are characterised by different shapes that are determined by the orientation

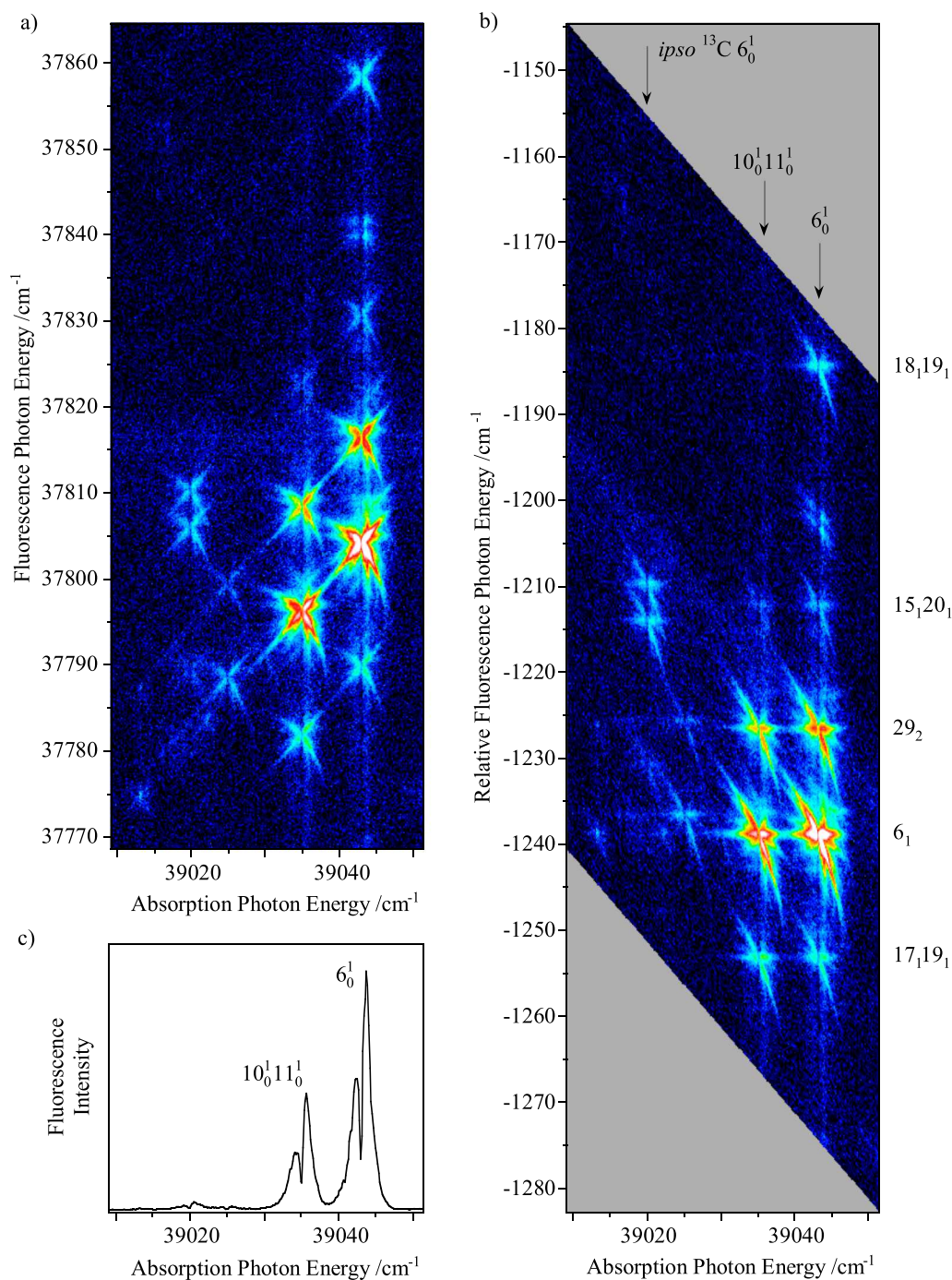


**Fig. 3.** (a) A 2D-LIF image of superphonically cooled fluorobenzene in the region of the  $6_0^1$  absorption and  $6_1^1$  emission. (b) A “skewed” version of the image shown in (a) such that horizontal lines correspond to constant  $S_0$  energy. Emission features from different  $S_1$  states that terminate in the same  $S_0$  vibration during the scan appear on a horizontal line in this image. The main  $^{12}\text{C}$  excitation transitions and terminating states are labelled. (c) The corresponding “LIF” spectrum, obtained by vertical integration of image (a).

of the transition dipole relative to the molecule’s Principle rotation axes. The Principle axes are conventionally labelled  $a$ ,  $b$  and  $c$ , where  $I_a > I_b > I_c$ ,  $I_x$  denoting the moment of inertia for rotation about the  $x$ -axis. An  $A$ -type contour, for example, arises when the transition dipole is parallel to the  $a$ -axis. In 2D-LIF the rotational structure

gives different shapes (2D contours) that depend on the orientation of the transition dipoles for both the excitation and emission steps, and these can be different. This is illustrated in Figure 4, which shows a  $3 \times 3$  “matrix” of images, corresponding to the 9 possible combinations of transition dipole direction pairs.

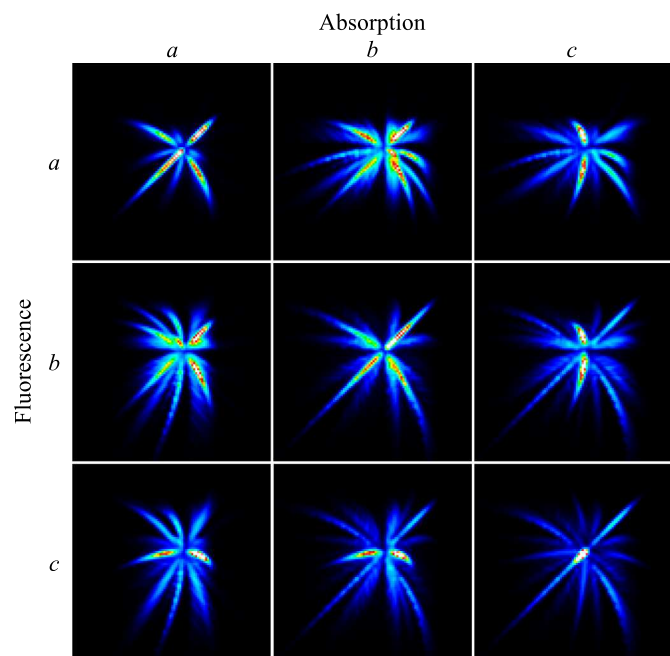


**Fig. 4.** Examples of the different shapes (2D contours) that can arise in 2D-LIF images as a result of the different combinations of transition dipole orientations for the excitation and emission steps. The simulations use the rotational constants of fluorobenzene [21] and are for a temperature of 10 K. The figure shows a  $3 \times 3$  “matrix” of images, corresponding to the 9 possible combinations of transition dipole direction pairs. The absorption and fluorescence transition dipole directions are labelled in the figure with reference to the Principal inertial axes of the molecule, *a*, *b* and *c*. For example, the three images in the column labelled *b* all correspond to an absorption transition dipole parallel to the *b*-axis. The upper image has the emission dipole direction parallel to the *a*-axis, the middle image has emission parallel to the *b*-axis, while the lower image has emission parallel to the *c*-axis.

One advantage of the 2D-LIF technique over conventional spectra is the ability to discern very weak features through the mind’s ability to recognise shapes in the image. Figure 3a illustrates this point. It shows a 2D-LIF image of fluorobenzene taken scanning a ca.  $40 \text{ cm}^{-1}$  wide segment in the region of the  $6_0^1$  absorption transition while monitoring emission near  $6_1^1$ . Numerous features, in the form of “crosses”, can be seen. The corresponding “LIF” spectrum, obtained by vertical integration of the image, is shown below it. We draw attention to the two features at an excitation energy of  $39\,025.0 \text{ cm}^{-1}$  in the image. The upper of the two features is readily discernible yet contributes only ca. 25% of the intensity to the very weak band seen in the “LIF” spectrum. We find that the wide dynamic range obtained in the images, as witnessed by this example, means that it is sometimes preferable to display them using a logarithmic scale.

In terms of limitations to the technique, the most obvious is that the species being studied must have a quantum yield for fluorescence that is sufficient to enable its emission to be detected. The signal level that is detectable in a given experiment also depends on the concentration

of the species under investigation and the efficiency of the fluorescence collection and detection. Scattered light can be the biggest limitation in this context, as it can determine the background signal level. A second issue to be aware of, particularly for high resolution fluorescence detection, is that the absorption transitions detected are limited to those that fluoresce in the spectral region monitored. The “LIF spectrum” determined from an image will have absorption features missing when they do not emit in the region monitored. For this reason, we recommend that those designing instruments consider incorporating the ability to monitor both high resolution and low resolution dispersed fluorescence simultaneously (i.e. two spectrometers), particularly where unknown samples are probed. Such a capability allows the experimenter to see where the bands being monitored in high resolution fit into the bigger picture of the overall fluorescence spectrum.

### 3 Examples of 2D-LIF

In this section we provide examples of the use of 2D-LIF to illustrate the diversity of its uses and applications to date. No doubt others will emerge as the technique becomes increasingly known and its use more widespread. We have divided the examples into two groups, defined by the resolution and spectral region monitored. The first group involves experiments that monitor a wide fluorescence spectral region with modest resolution while the second group involves experiments that monitor a narrow fluorescence spectral region with high resolution. As noted in Section 2, achieving high resolution and wide spectral coverage are to a large extent mutually exclusive due to the high dispersion associated with a high resolution spectrometer.

#### 3.1 Experiments monitoring fluorescence in a wide spectral region with modest resolution

##### 3.1.1 Identifying new species in a complex gas phase chemical environment

In their original paper, RSK describe their motivation in developing the 2D-LIF method as one of identifying and characterizing chemical species in complex environments [19]. (In their paper the term two-dimensional fluorescence (2DF) was used rather than 2D-LIF.) Their experiment involved searching for new chemical species produced in a supersonic expansion subjected to an electrical discharge. The discharge dissociates molecular species seeded in the carrier gas and the ensuing chemistry can lead to previously unobserved species. However, the new species being sought, which could be a neutral molecule, a radical or an ion, is present along with numerous other chemical species that have much higher concentrations. While the cooling associated with supersonic expansion simplifies spectra, there is nevertheless a plethora of transitions and identifying new (and even known) species becomes a difficult exercise. The 2D-LIF method takes advantage of the fact that the dominant species have known absorption and emission spectra. The authors noted that “Simultaneous

collection of a dispersed fluorescence spectrum for every step of the laser wavelength results in a two-dimensional spectrum of emission versus excitation wavelengths. This two-dimensional fluorescence (2DF) spectrum yields quick and intuitive assignments of a multitude of peaks in the separate fluorescence excitation and dispersed fluorescence spectra as belonging to the same species". The authors went on to demonstrate the technique for a discharge of  $\sim 0.1\%$  benzene in an argon expansion. Bands associated with  $C_2$  and  $C_3$  products dominate the image (Fig. 1) but the characteristic fingerprints of  $C_2$  and  $C_3$  allowed the identification of another unidentified species in the discharge that absorbs at 476 nm, which is, interestingly, coincident with one of the diffuse interstellar bands. In this application, the dispersed fluorescence dimension effectively provides a means to filter out certain species.

Schmidt and Kable have primarily used the 2D-LIF method as a sophisticated filter to identify and spectroscopically characterise new species produced in discharges, particularly key radical intermediates. These include the 1-phenylpropargyl radical [30,31], the *cis*- and *trans*-1-vinyl propargyl radicals [32], and various 1-indanyl-based resonance-stabilized radicals containing a hydroxyl group [33]. These authors presented a combined resonance enhanced multiphoton ionisation-time of flight mass spectrometry (REMPI-ToFMS) and 2D-LIF protocol to identify and spectroscopically characterise species formed in discharges [34]. They have also utilised the 2D-LIF technique for spectroscopic applications, identifying and assigning electronic band systems in  $C_2$ , including the first detailed report of the  $e^3\Pi_g - c^3\Sigma_u^+$  transition [35,36].

### 3.1.2 Spectroscopic studies of small molecules

Steimle and co-workers have studied a number of small molecules including the diatomics ThO [29] and SiO<sup>+</sup> [37] and the triatomic SiHD (monodeuterated silylene) [38] using 2D-LIF. While the motivation in the case of each molecule is different, the common thread of this work is the use of 2D-LIF to identify and isolate the LIF signal of interest from the multitude of other species present. In this context, their application of 2D-LIF is similar to that of Kable and Schmidt discussed in the previous section. As noted in Section 2, Steimle's group scans the fluorescence spectrometer synchronously with the laser, such that the laser remains at a fixed horizontal position at the detector, which is advantageous when scanning over a large excitation wavelength range. A 2D-LIF image from their paper on SiHD [38] is shown in Figure 5 to illustrate the type of image obtained with this approach.

This group has typically used a  $0.3\text{ cm}^{-1}$  pulsed dye laser coupled with a spectrometer with a resolution of 2 nm in the visible/near UV region (this corresponds to a fluorescence resolution of  $80\text{ cm}^{-1}$  at 500 nm). A particularly notable development in the case of the SiHD experiments is the coupling of 2D-LIF with a high resolution, cw laser source. This allowed LIF spectra of SiHD to be distinguished and recorded at a resolution of 200 MHz ( $0.007\text{ cm}^{-1}$ ) [38].

## 3.2 Experiments monitoring a narrow spectral region in fluorescence with high resolution

An issue with experiments utilizing high resolution in the fluorescence step is that only a small spectral region can be monitored, depending on the dispersion of the spectrometer and size of the detector (see Sect. 2). Consequently, applications in this regime are best focused on problems where the spectral region of interest is narrow and can be observed at a single (or small number of) spectrometer position(s).

### 3.2.1 The high sensitivity of 2D-LIF: spectral shifts of isotopomers in natural abundance

The 2D-LIF technique provides excellent sensitivity that derives from the substantially increased number of laser shots that can be averaged while measuring the fluorescence spectrum compared with scanning a spectrometer using photomultiplier detection. Nowhere is this more apparent than in the observation of isotopomers in natural abundance. In our original paper presenting the high resolution 2D-LIF technique applied to fluorobenzene, images revealed features arising from the  $^{13}\text{C}$  and  $^2\text{H}$  isotopomers in natural abundance [21]. The combined intensity of the  $0_0^0$  bands from the *ortho*, *meta* and *para*  $^2\text{H}$  isotopomers relative to the fluorobenzene origin band is 0.041%, demonstrating the sensitivity of the technique in being able to observe them. With a  $^{13}\text{C}$  natural abundance of  $\sim 1\%$ ,  $\sim 6\%$  of a fluorobenzene sample is expected to contain one of the  $^{13}\text{C}$  isotopomers, of which there are four depending on the site of the  $^{13}\text{C}$  relative to the fluorine atom: *ipso*, *ortho*, *meta* and *para*. The spectral shifts associated with the  $S_1-S_0$   $0_0^0$  transition for the four  $^{13}\text{C}$  isotopomers of fluorobenzene have been determined with the aid of ab initio calculations of the magnitude of the vibrational frequency changes on  $^{13}\text{C}$  substitution [23].

A potential extension of 2D-LIF from this work is the accurate determination of  $S_1$  and  $S_0$  vibrational frequencies for  $^{13}\text{C}$  substituted species. This provides a test of the accuracy of ab initio calculated vibrational force constants since the substitution of  $^{13}\text{C}$  for  $^{12}\text{C}$  does not change the force field but changes the vibrating mass and thus vibrational frequency. The image from an example of such an experiment is given in Figure 3, which shows a short scan near the  $6_0^1$  absorption transition of fluorobenzene while monitoring emission near  $6_1^1$ . Multiple weak features are seen. As noted in Section 2, transitions terminating in the same vibrational level lie on the same image "diagonal" and skewing the image such that this diagonal is horizontal facilitates identification of common terminating vibrations accessed from different  $S_1$  states. The corollary of this is that features that do not lie on the same horizontal line terminate in different states. Figure 3b shows the skewed version of Figure 3a. The strong absorption features at  $39035.0\text{ cm}^{-1}$  and  $39043.0\text{ cm}^{-1}$  display the behaviour discussed, with corresponding pairs of emission features appearing on the same horizontal line. Their  $S_0$  identity is indicated on the figure. They are clearly associated with the dominant component of the sample, in which the six C atoms are all  $^{12}\text{C}$ . However, the weak features at

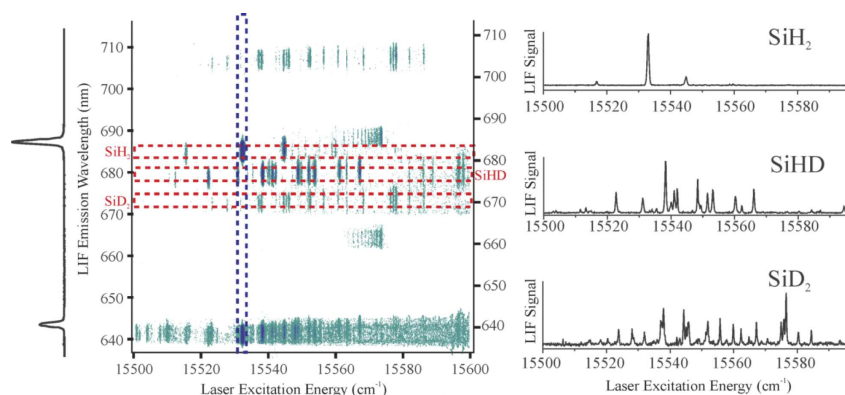


**Fig. 5.** A 2D-LIF image from the work of Steimle's group on SiHD, illustrating the type of image obtained when scanning the fluorescence spectrometer synchronously with the laser, such that the laser remains at a fixed position at the detector. Note the use of integration across different regions of the image to reveal spectra associated with different molecular species. (Reproduced from Ref. [38].)

$39\,019.9\text{ cm}^{-1}$  and  $39\,025.0\text{ cm}^{-1}$  in absorption terminate at different  $S_0$  energies. These features are associated with fluorobenzene with a single  $^{13}\text{C}$  replacing a  $^{12}\text{C}$ . Ab initio calculations can predict the frequency changes due to  $^{13}\text{C}$  substitution at the various positions in the aromatic ring and hence the spectral shifts expected for each isotopomer for the vibrations observed in this region. Such calculations indicate that the feature at  $39\,019.9\text{ cm}^{-1}$  is due to  $6_0^1$  for *ipso*- $^{13}\text{C}$ . The image allows isotopic frequency shifts in both  $S_1$  and  $S_0$  to be determined.

The vibrations of phenol have been used as a benchmark for testing the harmonic frequencies obtained from ab initio calculations for both  $S_0$  and  $S_1$  states [39]. Phenol has been studied by dispersed fluorescence spectroscopy previously [39], and consequently would appear to be a prime candidate for a future 2D-LIF study of the  $^{13}\text{C}$  isotopomers to determine their vibrational frequencies and thereby provide an important test of the calculated force fields.

### 3.2.2 Determining polyatomic rotational constants with high precision using lasers of modest resolution: a case for room temperature spectroscopy

Molecular spectra measured at room temperature suffer from congestion due to the large number of quantum states populated. Excitation from thermally populated vibrational states leads to sequence structure and hot bands, while excitation from thermally populated rotational states leads to the rotational contours associated with vibrational bands extending for  $30\text{ cm}^{-1}$  or more. It is now almost 40 years since molecular spectroscopy was revolutionised by the introduction of supersonic expansion as a means of cooling gas phase samples to ultra-low temperatures, thereby largely eliminating thermal congestion and greatly simplifying spectra [40]. Molecular spectra are now routinely measured at temperatures of a few Kelvin.

The rotational constants, which relate to a molecule's geometry, are key spectroscopic parameters. However, somewhat perversely, having population confined to low rotational states limits the accuracy with which these

constants can be determined using typical commercial nanosecond laser systems. High resolution lasers are required to obtain spectra with sufficient structure to be able to extract rotational constants through fitting the contour or, preferably, to observe individual rotational lines.

2D-LIF using warmer samples (e.g. room temperature) provides an interesting alternative to supersonic cooling to obtain data from which rotational constants can be extracted with high precision using a typical commercial nanosecond laser source. In the case of 2D-LIF, spectral congestion is simplified through the use of the fluorescence spectral dimension rather than cooling, with features that overlap in the usual laser induced fluorescence spectrum separated in the 2D-LIF image. A significant advantage of 2D-LIF imaging is that the rotational contours separate into their constituent branches, which facilitates the determination of the rotational constants. Since only a narrow region of fluorescence need be monitored to capture the 2D rotational contour, this application meshes well with the constraints of high resolution 2D-LIF experiments.

As an example of this application, we studied the  $0_0^0$  band region of fluorobenzene at room temperature. The 2D-LIF image is shown in Figure 2 [21]. The study illustrates the extent to which the 2D-LIF approach can remove spectral overlap, particularly from sequence bands, and hence reveal the rotational structure at high  $J$  ( $J$  denotes the total angular momentum quantum number). This is the key to this application: since the spectra measure differences in  $J$  of, for example,  $+1$  in the case of an  $R$  branch and the energy scales approximately as  $J^2$  at high  $J$ , the position of the  $R$  branch rotational feature from the band origin scales linearly with  $J$ . The higher the  $J$  measured, the more accurately the corresponding rotational constants can be determined for a given resolution. Comparing the 2D-LIF spectral image and the (1D) LIF spectrum (lower panel in Fig. 2) reveals the clear advantages of the 2D-LIF technique; 2D-LIF separates the contributions of sequence bands and different rotational branches. This separation makes it possible to observe much higher rotational states than is possible in an LIF

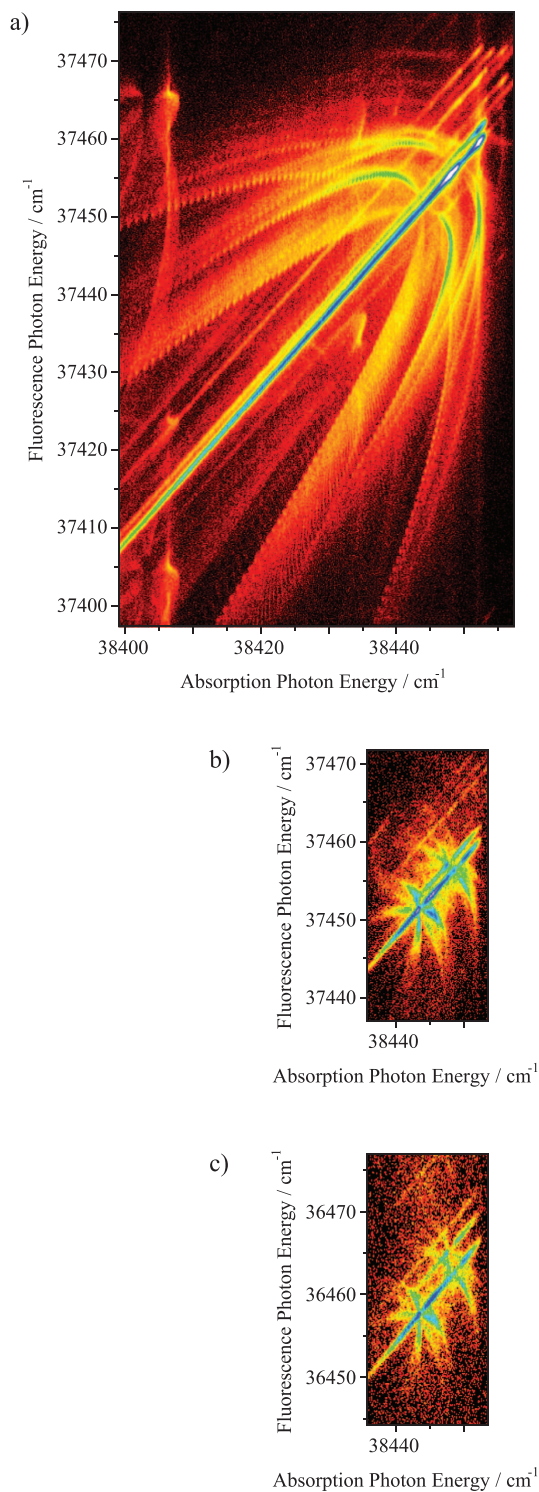


**Fig. 6.** 2D-LIF images following excitation of the overlapped  $6_0^1 11_1^1 / 6_0^1 16_1^1$  absorption features: (a) the image for a room temperature sample showing transitions terminating in the  $1_1 11_1 / 1_1 16_1$  levels; (b) as for (a) but for a supersonically cooled sample; and (c) the image for a supersonically cooled sample terminating in the  $1_2 11_1 / 1_2 16_1$  levels [47]. The panels have their  $x$ -axes aligned. The  $1_1^0 6_0^1 11_1^1 / 1_1^0 6_0^1 16_1^1$  and  $1_2^0 6_0^1 11_1^1 / 1_2^0 6_0^1 16_1^1$  fluorescence transitions are sufficiently split to separate the  $6_0^1 11_1^1$  and  $6_0^1 16_1^1$  absorption bands, allowing the previously unknown  $\nu_{11}$   $S_1$  frequency to be determined.

spectrum. A further advantage of the 2D-LIF image is that weak rotational transitions that are not apparent in the LIF spectrum are revealed in the rich rotational structure observed, aiding the accurate and unambiguous determination of the rotational constants.

Fitting the features in Figure 2 gives rotational constants  $A = 5345.7 \pm 0.1$  MHz,  $B = 2539.6 \pm 0.2$  MHz and  $C = 1721.4 \pm 0.1$  MHz. These are of a precision comparable with that achieved for a supersonically cooled sample of the related mono substituted methylbenzene (i.e. toluene) using a ca. 1 MHz line width laser [41] despite the fluorobenzene experiment using a laser of line width ca.  $10^4$  MHz.

### 3.2.3 Detangling overlapping vibronic bands through anharmonic shifts

The accidental overlap of vibrational bands in electronic spectra can prevent an accurate determination of the vibrational frequencies and associated rotational constants. Such a situation arises in benzene, whose  $S_1$ – $S_0$  ( $^1B_{2u} \leftarrow ^1A_{1g}$ ) transition has received significant attention because it is both the “parent” for aromatic  $\pi^* \leftarrow \pi$  transitions and the textbook example of an electronically forbidden transition that is observed due to Herzberg–Teller coupling. The  $6_0^1 11_1^1$  and  $6_0^1 16_1^1$  transitions are very strongly overlapped and as a result the  $S_1$  value for  $\nu_{11}$  has only been reported to within a range of  $3 \text{ cm}^{-1}$  ( $515$ – $518 \text{ cm}^{-1}$ ) [42,43]. This can lead to limitations in the parameters that can be extracted from an analysis of benzene spectra to determine, for example, rotational and vibrational populations. As an illustration of this, benzene has been used as a spectroscopic probe of the dynamics of a molecule leaving a liquid surface under vacuum as its absorption spectrum can be used to reveal which rotational and vibrational states are populated during the evaporation process [44,45]. However, the overlapping absorption of the  $6_0^1 11_1^1$  and  $6_0^1 16_1^1$  transitions hampers the determination of rotational temperatures and vibrational populations for the  $11_1$  and  $16_1$  levels.

The 2D-LIF technique provides a means to separate these strongly overlapped transitions through monitoring emission to levels where the vibrational anharmonicity helps to split them. In the case of the  $6_0^1 11_1^1$  and  $6_0^1 16_1^1$  transitions, fluorescence to terminating levels involving combinations with  $\nu_1$  can split this energetic degeneracy and separate the two absorption transitions. The difference in energy between the two transitions  $1_1^0 6_0^1 11_1^1$  and  $1_1^0 6_0^1 16_1^1$  is increased by  $x_{1,11} - x_{1,16}$  compared with the  $6_0^1 11_1^1$  and  $6_0^1 16_1^1$  transitions, where  $x_{ij}$  is the anharmonicity constant for vibrations involving  $\nu_i$  in combination with  $\nu_j$ . Miani et al. calculated  $x_{ij}$  values for benzene using density functional theory, with their results indicating that the expected change in separation is ca.  $1.1$ – $1.5 \text{ cm}^{-1}$  [46]. This small splitting of the  $1_1^0 6_0^1 11_1^1$  and  $1_1^0 6_0^1 16_1^1$  bands is enough to separate the  $6_0^1 11_1^1$  and  $6_0^1 16_1^1$  transitions when a high resolution spectrometer is used for the fluorescence dimension.

On the basis of this predicted splitting, Maselli, using the apparatus in our laboratory, measured 2D-LIF images

of the ( $6_0^1 11_1^1$ ,  $1_1^0 6_0^1 11_1^1$ ) and ( $6_0^1 16_1^1$ ,  $1_1^0 6_0^1 16_1^1$ ) benzene features using both room temperature and supersonically cooled samples [47]. The images are reproduced in Figure 6. We have taken a further image of the ( $6_0^1 16_1^1$ ,  $1_2^0 6_0^1 16_1^1$ ) feature. The  $1_1^0 6_0^1 11_1^1$  and  $1_1^0 6_0^1 16_1^1$  transitions are split by  $1.16 \text{ cm}^{-1}$ , which is sufficient to separate the  $6_0^1 11_1^1$  and  $6_0^1 16_1^1$  bands, and the separation is further enhanced for the  $\nu_1 = 2$  combination. The previously undetermined  $\nu_{11} S_1$  frequency is found to be  $517.2 \text{ cm}^{-1}$  [47].

### 3.2.4 Application to van der Waals molecules

van der Waals molecules (also referred to as van der Waals complexes) are comprised of stable molecular and/or atomic components held together by intermolecular forces. They provide a means by which these weak intermolecular interactions can be studied using the precision of gas phase spectroscopic techniques. van der Waals molecules are formed as something of a “by-product” of supersonic expansion cooling and since the proliferation of this technology from the early 1980s have become a standard means by which to explore intermolecular interactions [40]. The weak van der Waals bonds give rise to low frequency vibrations (typically well below  $100 \text{ cm}^{-1}$ ) and so match well the limited spectral region observed in high resolution 2D-LIF experiments. A particular advantage of the 2D-LIF technique in this application is that it provides a window on the van der Waals vibrations in both the ground and excited electronic states. There is a paucity of data concerning van der Waals vibrations in the ground electronic state, for which ab initio calculations are most easily and accurately performed.

An example of a 2D-LIF image illustrating structure associated with van der Waals molecules is shown in Figure 7, which shows the results of a laser scan in the region near the fluorobenzene  $0_0^0$  band [22]. The  $S_0$  and  $S_1$  van der Waals vibrational frequencies are similar and there is limited geometry change between the two electronic states along the intermolecular axes, so the Franck-Condon factors strongly favour  $\Delta v = 0$  transitions. The strongest 2D-LIF features involve absorption via transitions of the type  $vdW_0^n$  followed by emission  $vdW_n^n$ , where  $vdW$  indicates any one of the van der Waals vibrations. These features are displaced vertically below the image diagonal by the ground state frequency of  $vdW_n$ , resulting in a near-horizontal series of features in the image for a particular van der Waals complex. Figure 7 illustrates this and also shows the distinctive 2D shapes that are displayed by the different species. Substituted benzenes, for example, typically show distinct “crosses” for the Franck-Condon allowed bands. When complexed with Ar, they display a much smaller feature with a distinctive central “stripe” due to the presence of a strong  $Q$  branch. The aromatic- $\text{Ar}_2$  complexes have a different shape again. This allows bands associated with the different van der Waals complexes to be readily distinguished from each other and from the bare parent.

The case of toluene-Ar is particularly interesting because the bands associated with the methyl torsional motion (i.e. internal rotation of the methyl group) and van der Waals vibrations are both low frequency and appear

in the narrow fluorescence window. The 2D-LIF image allowed the  $S_0$  van der Waals and methyl rotor levels to be observed for the first time [24]. Importantly, correlations between the  $S_0$  and  $S_1$  states seen in the 2D-LIF images led to a reassignment of the features in the  $S_1 \leftarrow S_0$  excitation spectrum and revealed that there are significant changes in the methyl torsion levels in the complex compared with those in bare toluene, particularly when low quanta are present in the torsional motion, in contrast to the conclusions of an earlier report based on REMPI spectra [48].

### 3.2.5 Methyl internal rotation and its interaction with molecular vibrations

Perhaps the most significant contribution made using the high resolution 2D-LIF imaging technique to date is in the area of methyl internal rotation, which is also referred to as methyl torsion, and consequently we present this section in more detail. Internal rotation is an example of a so-called large amplitude motion [49,50]. Large amplitude motions contrast with the usual vibrations of the molecule, which involve comparatively small, near harmonic excursions about an equilibrium geometry [51].

Internal rotation can be regarded as being well understood given that there is a long history of successful analysis of rotational spectra measured in the microwave and adjacent spectral regions, with the computer codes required being highly developed and freely available [52–54]. These analyses consider the problem in terms of the interaction of internal rotation of the methyl group with overall rotation of the molecule [52,55]. It is assumed that the methyl rotation is independent of the molecular vibrations, at least for the lower torsional states [49,55–57]. Observed line positions are fit with a precision of ca. 1 part in  $10^8$  [52,55]. The parameters extracted provide physical insights, such as the magnitude of the barrier to the torsional motion. The fact that the models successfully fit a plethora of lines with a precision of ca. 1 part in  $10^8$  provides compelling evidence for the validity of the underlying assumptions. Furthermore, there are now many molecules, in particular substituted toluenes, for which the torsional modes have been observed directly in electronic spectra and their energies have, for the most part, been successfully reproduced assuming that the torsional motion is unaffected by the small amplitude vibrations [58–74].

Methyl rotation is an excellent candidate for examination using high resolution 2D-LIF because the torsional energies can be quite low. In the case where there is no barrier to methyl rotation, the energies are given by  $F \underline{m}^2$ , where  $F$  is the rotational constant associated with the internal rotation and  $\underline{m}$  is the quantum number associated with its angular momentum [49,75].  $\underline{m}$  takes values of  $0, \pm 1, \pm 2, \dots$ , with the positive and negative values denoting different rotation directions, i.e. clockwise versus anti-clockwise.  $F$  for the  $-\text{CH}_3$  moiety is typically  $\sim 5.3 \text{ cm}^{-1}$ , and thus this free rotor will have energies below  $100 \text{ cm}^{-1}$  for  $|\underline{m}| \leq 4$ . The introduction of a small barrier to the internal rotation produces so-called hindered rotor states, labeled  $m$ , where generally  $m = |\underline{m}|$ ,

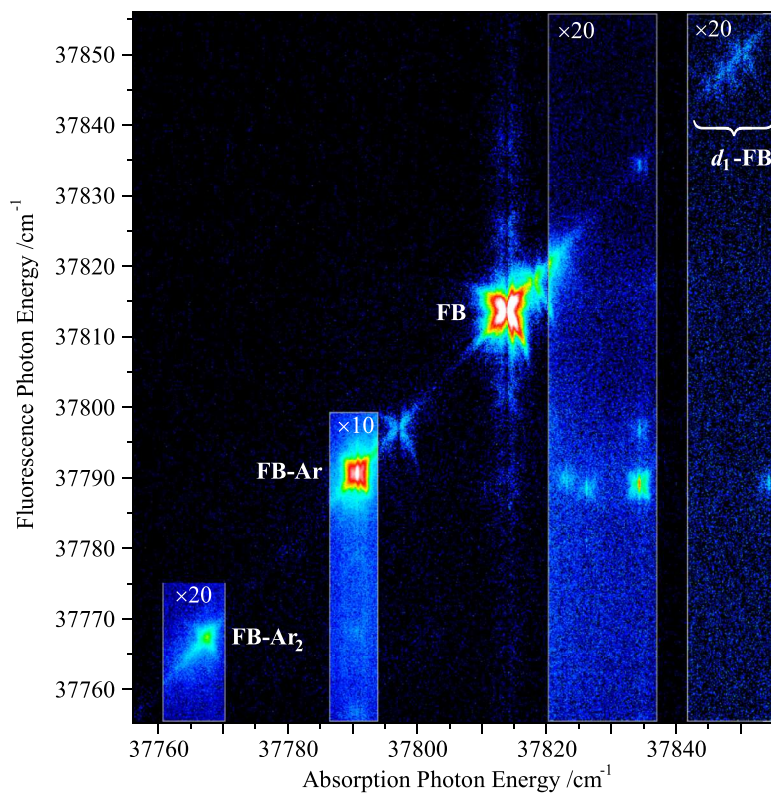


**Fig. 7.** A 2D-LIF image of a laser scan of fluorobenzene seeded in a supersonic expansion of argon in the region near the  $0_0^0$  band. Features associated with fluorobenzene and the fluorobenzene-Ar and fluorobenzene-Ar<sub>2</sub> van der Waals molecules are seen. Note the different shapes associated with the 2D rotational contours for the different molecular species. (Adapted from Ref. [22].)

but does not change these energies greatly [49,75] and so the ca.  $90\text{ cm}^{-1}$  wide fluorescence window on our instrument can observe a number of transitions associated with the methyl rotor simultaneously. (In the case of molecules with a high barrier (say  $> 100\text{ cm}^{-1}$ ), the separation between torsional bands may become large enough that the fluorescence has to be collected in several laser scans using different fluorescence windows.)

The presentation here focuses on an investigation of methyl rotation in toluene. With the phenyl frame to which the methyl is attached having  $C_{2v}$  symmetry, the methyl rotation involves a torsional potential of height  $V_6$  that repeats six times during a  $360^\circ$  rotation. Six-fold barriers are generally quite low and in toluene the methyl is almost a free rotor [41,55]. Consequently, the assumption that the vibrations can be ignored, which is regarded as valid when there is a large frequency difference between the small amplitude normal vibrations and the large amplitude methyl torsion, should be well met here since nowhere is this mismatch in frequencies more apparent than when the methyl is a free rotor [49]. Our study of toluene was motivated originally to take advantage of (a) the high sensitivity of 2D-LIF to observe  $m > 4$  states, which had not been observed previously [74,76], and (b) high fluorescence resolution to better determine  $S_0$  band positions given the low resolution ( $\sim 14\text{ cm}^{-1}$ ) of previous reports [74]. Toluene, being the “parent” for methyl rotation in substituted toluenes, has been well studied and the

key constants determined from the analysis of microwave and rotationally resolved LIF spectra are summarised in Table 1 [41,55,74]. The precision of these constants leads to high precision in the predicted  $m$  state energies and 2D-LIF provides a means to confirm these predicted torsional energies.

Figure 8a shows the 2D-LIF image predicted for the first  $215\text{ cm}^{-1}$  of the  $S_1 \leftarrow S_0$  transition of toluene using the constants determined from previous studies (Tab. 1). Our experimental 2D-LIF image covering the same region as the predicted image is shown in Figure 8b [28]. We were anticipating excellent correspondence between the experimental and calculated images, however, even a superficial assessment indicates that while the differences are modest in the region from  $0_0^0$  to  $0_0^0 + 100\text{ cm}^{-1}$ , they become substantial above  $0_0^0 + 100\text{ cm}^{-1}$  where the  $m > 4$  torsional states lie.

It transpires that the reason for the mismatch is that the methyl internal rotation is strongly influenced by the lowest vibrational mode,  $M_{20}$ , whose frequency is  $204\text{ cm}^{-1}$  in  $S_0$  and  $140\text{ cm}^{-1}$  in  $S_1$  [27,28]. This mode involves an out-of-plane wagging of the methyl group. The interaction between torsion and vibration has been observed in several substituted toluenes previously, so its presence in toluene is not a complete surprise; indeed, higher order torsion-vibration coupling interactions have been observed in this molecule [25]. However, in the previous studies, the torsion-vibration interaction has been considered simply

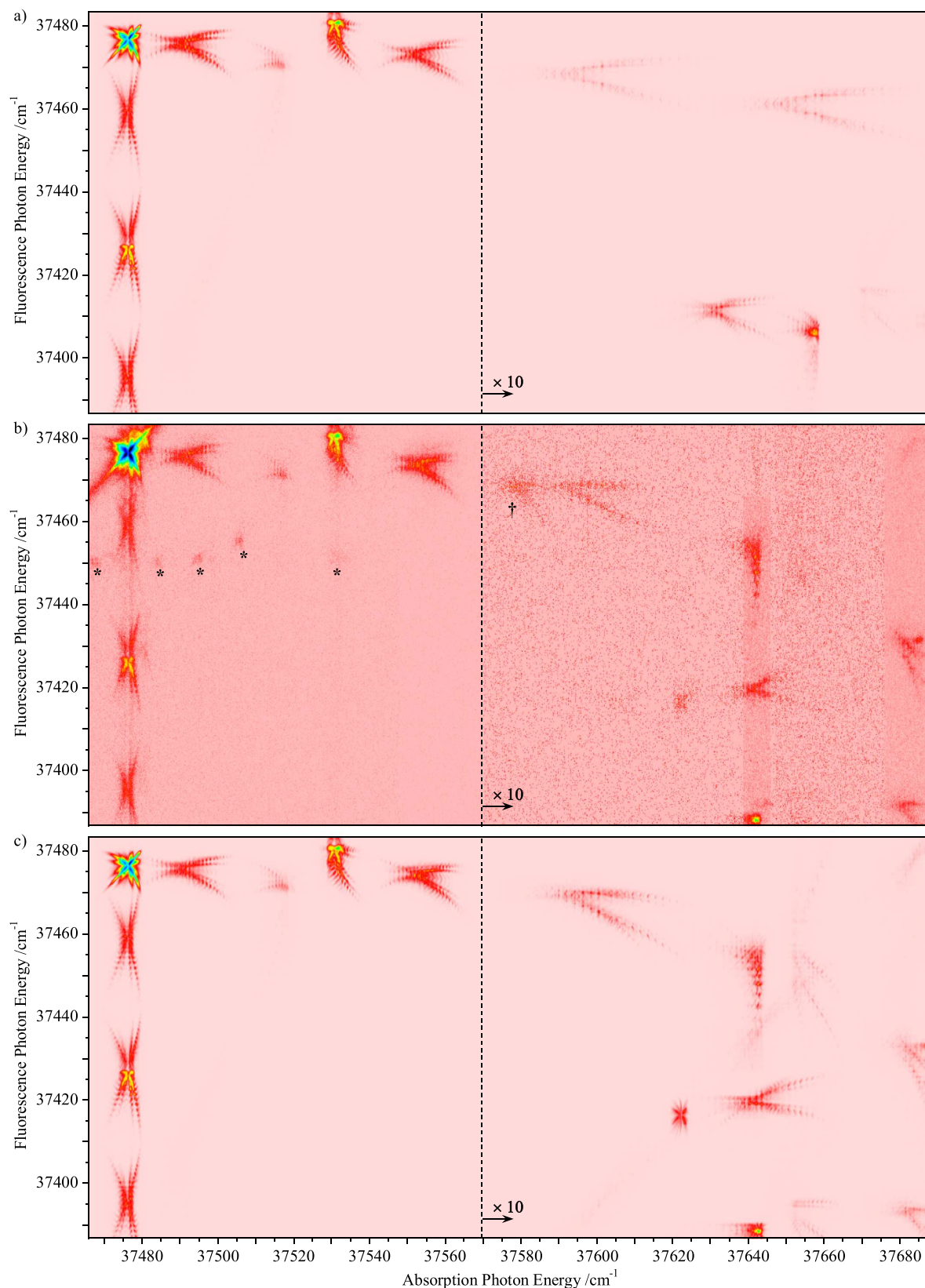


**Fig. 8.** (a) The 2D-LIF image predicted for the first 215 cm<sup>-1</sup> of the S<sub>1</sub> ← S<sub>0</sub> transition of toluene using the original constants (Tab. 1). (b) The experimental 2D-LIF image covering the same region as the predicted image shown in (a) (Adapted from Ref. [28]). The asterisks denote bands due to toluene-Ar van der Waals molecules [24]. The † symbol indicates the (m<sub>2</sub><sup>5</sup>, m<sub>5</sub><sup>5</sup>) hot band transition which is not included in the simulated images. (c) The 2D-LIF image predicted for the first 215 cm<sup>-1</sup> of the S<sub>1</sub>-S<sub>0</sub> transition of toluene using revised constants (Tab. 1).

**Table 1.** Constants used to determine torsional band positions as determined from the analysis of microwave and rotationally resolved LIF spectra compared with those determined using 2D-LIF.

Constant	No torsion-vibration interaction		Including torsion-vibration interaction	
	S <sub>0</sub> value <sup>a</sup> (cm <sup>-1</sup> )	S <sub>1</sub> value <sup>b</sup> (cm <sup>-1</sup> )	S <sub>0</sub> value <sup>c</sup> (cm <sup>-1</sup> )	S <sub>1</sub> value <sup>d</sup> (cm <sup>-1</sup> )
$F$	5.466956	5.298	5.50	5.455
$dF^e$	–	–0.008	0	–0.0013
$V_6$	(–)4.83783617 <sup>f</sup>	–26.376	1.57	–5.59
$V_{T-v}$	–	–	15.55	21.12

<sup>a</sup> Reference [55].

<sup>b</sup> Reference [41].

<sup>c</sup> Reference [27].

<sup>d</sup> Reference [28].

<sup>e</sup>  $dF$  is a centrifugal distortion term for the methyl rotor [41]. It modifies the free rotor energy expression so that it is  $E(\underline{m}) = \underline{m}^2(F + \underline{m}^2 dF)$ .

<sup>f</sup> The bracketed minus sign indicates that the authors were unable to determine the sign of  $V_6$ , however, the 2D-LIF image shows it to be negative.

as a local perturbation between pairs of states and coupling terms were determined based on this analysis. Table VIII of reference [72] provides a summary of such terms.

A limitation of previous LIF and dispersed fluorescence studies of methyl torsional states has been the precision with which band origins could be determined because the rotational structure of torsional bands can be extensive. Band positions have been taken simply as the wavelength of maximum intensity. However, the 2D-LIF image reveals unique shapes for the features, inviting a better approach. We fit calculated 2D rotational contours to these features, which allows the band positions to be extracted with an uncertainty of ca.  $\pm 0.1$  cm<sup>-1</sup>, a significant improvement on previous measurements. The enhanced precision with which the band positions are determined and the observation of the 2D rotational structure make it possible to see that the effects of the interaction of the torsional motion with the methyl wagging vibration are more widespread than simply a local perturbation. The interaction not only moves bands, it also alters the rotational structure, and this can be subtle or substantial, as shown in Figure 9. We find that the torsion-vibration interaction affects the torsional and torsion-vibration states well beyond local perturbations and has wide ranging implications for the constants extracted from conventional analyses [27,28,77]. In fact, the torsional structure has to be solved with the torsion-vibration interaction explicitly included for all states in order to properly reproduce the 2D-LIF image. The resulting calculated 2D-LIF image is shown in Figure 8c. The calculated image now accurately reproduces the experimental one.

The constants required to reproduce the torsion and torsion-vibration band positions observed in S<sub>0</sub> and S<sub>1</sub> toluene are remarkably different to those determined previously, as seen in Table 1. The inclusion of torsion-vibration coupling causes the value for the torsional barrier,  $V_6$ , to be reduced and the value for the torsional rotation constant,  $F$ , to be increased. The determination of torsional barriers is one of the key aims of experiment in this field [49,57]. It is particularly disturbing that the constants required to reproduce the torsion and torsion-vibration band positions in the 2D-LIF image are so different to those determined by analysis of the rotational

spectrum [55]. The fit to the microwave (S<sub>0</sub>) data involved 372 lines covering four internal rotation (i.e.  $m$ ) states using 28 parameters and resulted in a root mean square (rms) deviation between the calculated and observed lines of only 7 kHz. In the excited electronic state, S<sub>1</sub>, the fit involved 385 lines covering three  $m$  states using 6 parameters. The lines were fit with an rms of 3 MHz (0.0001 cm<sup>-1</sup>;  $1 \times 10^{-6}$  nm). How is it that the constants determined fail to detect the vibrational influences so clearly evident in the 2D-LIF image?

To explore this issue we undertook a new analysis of the microwave data, this time incorporating the torsion-vibration interaction that was required to reproduce the 2D-LIF image (Fig. 8c). *We found that by including torsion-vibration coupling the lines could be fit to the same precision as previously reported without this coupling [77].* In fact, we demonstrated that the rotational lines can be fit using a broad range of values for the torsion-vibration coupling constant. It transpires that, at least for the low  $m$  levels involved, the rotational line data can be modelled equally precisely using two different models. Crucially, however, the constants extracted are different and their interpretation provides a different physical picture in the two cases. While there are significant changes in many of the higher order constants, the most important changes are in the low order constants as these relate to physically meaningful parameters such as the molecule's geometry.

In summary, the capabilities afforded by the 2D-LIF technique have provided a unique window into the behaviour of the methyl rotor in toluene. Unexpectedly, this has shown that the usual assumption that torsion and small amplitude vibrations are decoupled is incorrect in this case. We say “unexpectedly”, since the toluene rotational line data for both S<sub>0</sub> and S<sub>1</sub> have been well fit previously using models that assume that torsion and small amplitude vibrations are decoupled [41,55]. A re-examination of the toluene microwave data revealed that such data are in fact not sensitive to this interaction [77]. This leads to the obvious question of whether this interaction is present in other molecular systems and, hence, how reliable are the geometries implied by the constants extracted from the analysis of microwave data for these types of molecules? It is clear that the high resolution

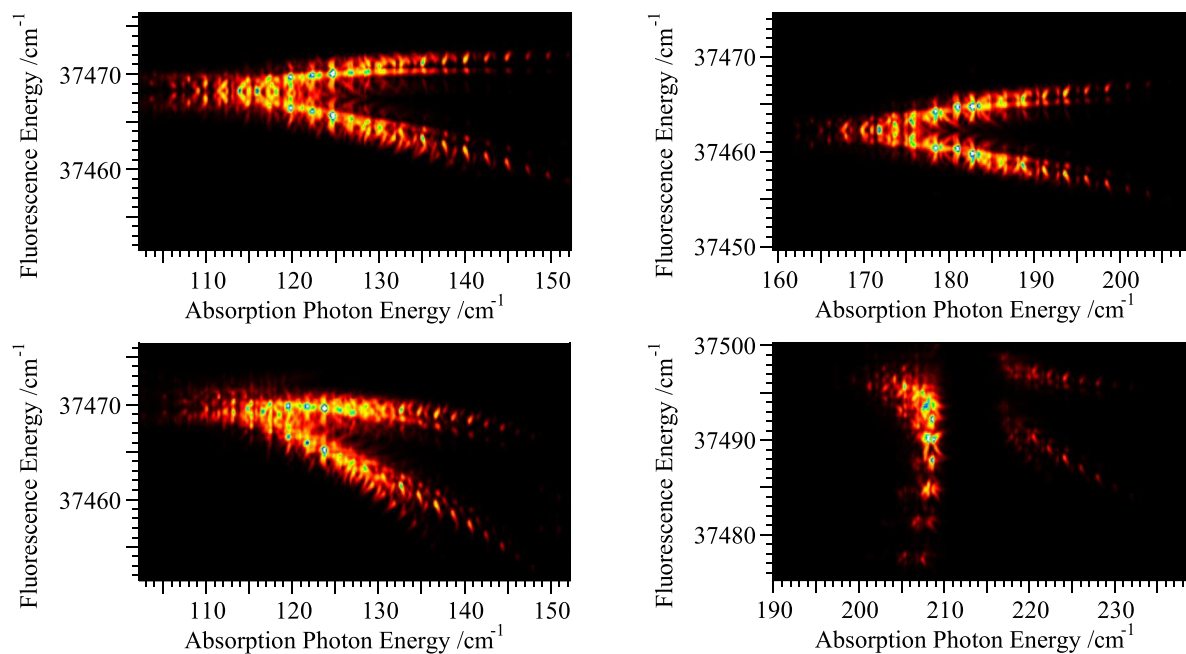


**Fig. 9.** Left hand panels: a comparison between the 2D rotational contour calculated for the  $(m_1^5, m_5^5)$  feature in toluene with (lower panel) and without (upper panel) the torsion-vibration interaction. For this band the changes are subtle as the interaction occurs over a large energy gap. Right hand panels: a comparison between the 2D rotational contour for the  $(m_0^{6(\pm)}, m_6^{6(\pm)})$  feature with (lower panel) and without (upper panel) the torsion-vibration interaction. Here the states are close-lying and are moved substantially by the torsion-vibration interaction; the rotational contour is unrecognisable from the contour without the interaction.

2D-LIF approach will be central to exploring this issue because it is able to provide a window on the torsional states directly, specifically their energies and rotational structure.

In this context, we show in Figure 10, a 2D-LIF image of the  $(m_1^4, m_4^4)$  torsional band of toluene taken with a commercial laser of line width ca.  $0.07 \text{ cm}^{-1}$ . The image reveals that improving the line width in the excitation step also simplifies the fluorescence step because the narrower laser excites fewer states, leading to less congestion in emission. Analysis of such images indicates that they will allow rotational constants to be extracted with a precision of ca. 1 MHz, pushing the 2D-LIF approach towards the realm previously requiring boutique high resolution laser systems. Such images can provide an unprecedented window into torsion-vibration interactions in toluene and related molecules.

## 4 Future developments

In this section we discuss some of the potential future directions that we envisage for 2D-LIF. An obvious area involves improvements in spectral resolution in both the excitation and emission dimensions. With the spectral separation and simplification provided by the fluorescence dimension, we envisage that rotational constants could be obtained with a precision comparable to that currently requiring specialist MHz line width laser systems. Moreover, an increase in the fluorescence resolution to

$<0.1 \text{ cm}^{-1}$  is entirely feasible given the resolution of spectrometers that were used in the pre-laser era for measuring absorption spectra [78]. There is a genuine possibility that 2D-LIF could provide a resolution comparable to that obtained with the multiple laser technique of stimulated emission pumping (SEP) [79] to probe spectroscopic structure in the ground electronic state, with a 2D advantage that would be difficult to realise with SEP.

A second straightforward modification of the technique involves the addition of time resolution to the fluorescence detection step. Image intensifiers can be gated, with gate widths of 5 ns commercially advertised. We envisage recording the fluorescence at each laser wavelength at a number of time slices, providing a three dimensional view of the intensity (intensity versus laser wavelength, fluorescence wavelength and time), giving a unique window on photophysical and photochemical processes.

The final potential modification that we consider is that of mass selectivity. Time of flight mass spectrometry (ToFMS) is routinely coupled with resonance enhanced multiphoton ionisation (REMPI) to allow the identity of ionised species to be determined and thereby assign the molecule responsible for an absorption feature in the resonant excitation step [80]. Indeed, Schmidt and Kable and their co-workers have presented a protocol for utilising REMPI-ToFMS with 2D-LIF to identify and subsequently characterise radicals produced in discharges [34]. A natural extension is for the two measurements to be combined into a single experiment. When a pulsed laser is used for the laser excitation step in 2D-LIF experiments, some of

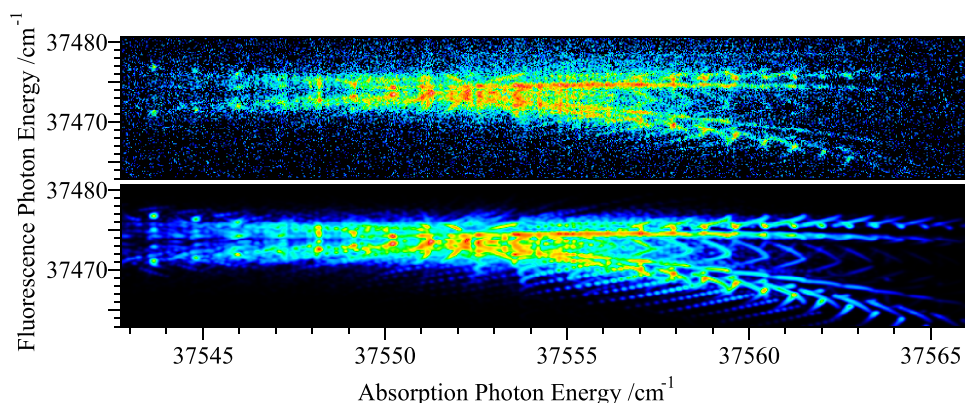


**Fig. 10.** Upper panel: a 2D-LIF image of the ( $m_4^4, m_4^4$ ) torsional band of toluene taken with a laser line width of ca.  $0.07 \text{ cm}^{-1}$ . The fluorescence resolution is ca.  $0.3 \text{ cm}^{-1}$ . Lower panel: the calculated image (incorporating torsion-vibration coupling) for comparison.

the excited molecules will be ionised by absorption of a second photon, while some will emit and contribute to the fluorescence signal. There is thus an opportunity to simultaneously determine the mass of the emitting species by mass analysis of the ions produced. By recording the entire mass spectrum [11] and dispersed fluorescence image simultaneously, excitation features, and by extension fluorescence features, can be assigned to a particular molecular species. As an extension of this approach, a second laser could be introduced for the ionisation step when fragmentation of the ionised species is an issue at the photon energy of the first laser.

## 5 Summary, conclusions and the future

The addition of the second dimension, the wavelength at which excited states emit, adds significantly to the information that can be extracted from the usual LIF spectrum. It allows overlapping absorption features, whether they originate from the same molecular species or from different molecules in a mixture, to be associated with their appropriate “parent” state and/or molecule. While the first gas phase version of the technique was published a decade ago, the technique is in its infancy, having been exploited by only a few groups to date. However, its potential is significant, and as we have shown it has already provided new insights into an old problem, that of methyl torsion. The future for the technique is bright and it is our hope that this brief overview illustrating the advantages of the technique will encourage more groups to take it up.

We thank Dr. Ula Alexander who worked on the 2D-LIF apparatus during its early development in our laboratory and Ms Edwina Virgo who recorded the high resolution image of toluene shown in Figure 10 and contributed to the toluene internal rotation work.

## Author contribution statement

This review was prepared jointly by the two authors.

## References

1. W.F. Reynolds, R.G. Enríquez, *J. Nat. Prod.* **65**, 221 (2002)
2. P. Giraudeau, L. Frydman, *Annu. Rev. Anal. Chem.* **7**, 129 (2014)
3. A.H. Kwan, M. Mobli, P.R. Gooley, G.F. King, J.P. Mackay, *FEBS J.* **278**, 687 (2011)
4. *Coherent multidimensional optical spectroscopy*, (ACS Publication, 2009), Vol. 42, pp. 1207–1469
5. L.K. Iwaki, D.D. Dlott, *J. Phys. Chem. A* **104**, 9101 (2000)
6. M. Cho, *Chem. Rev.* **108**, 1331 (2008)
7. P.C. Chen, *Appl. Spectrosc.* **70**, 1937 (2016)
8. D.M. Jonas, *Annu. Rev. Phys. Chem.* **54**, 425 (2003)
9. M.F. DeCamp, L.P. DeFlores, K.C. Jones, A. Tokmakoff, *Opt. Express* **15**, 233 (2007)
10. J.C. Dean, S. Rafiq, D.G. Oblinsky, E. Cassette, C.C. Jumper, G.D. Scholes, *J. Phys. Chem. A* **119**, 9098 (2015)
11. K. Matthíasson, H. Wang, Á. Kvaran, *J. Mol. Spectrosc.* **255**, 1 (2009)
12. G. Weber, *Nature* **190**, 27 (1961)
13. I.M. Warner, J.B. Callis, E.R. Davidson, G.D. Christian, *Clin. Chem.* **22**, 1483 (1976)
14. H. Anzai, N.K. Joshi, M. Fuyuki, A. Wada, *Rev. Sci. Instrum.* **86**, 014101 (2015)
15. C.S. Parmenter, M.W. Schuyler, *J. Chem. Phys.* **52**, 5366 (1970)
16. J.M. Blondeau, M. Stockburger, *Ber. Bunsenges. Phys. Chem.* **75**, 450 (1971)
17. C.S. Parmenter, *Adv. Chem. Phys.* **22**, 365 (1972)
18. A.E.W. Knight, C.S. Parmenter, M.W. Schuyler, *J. Am. Chem. Soc.* **97**, 1993 (1975)
19. N.J. Reilly, T.W. Schmidt, S.H. Kable, *J. Phys. Chem. A* **110**, 12355 (2006)
20. H. Neij, B. Johansson, M. Aldén, *Combust. Flame* **99**, 449 (1994)
21. J.R. Gascooke, U.N. Alexander, W.D. Lawrance, *J. Chem. Phys.* **134**, 184301 (2011)
22. J.R. Gascooke, U.N. Alexander, W.D. Lawrance, *J. Chem. Phys.* **136**, 134309 (2012)
23. J.R. Gascooke, W.D. Lawrance, *Chem. Phys. Lett.* **555**, 38 (2013)

24. J.R. Gascooke, W.D. Lawrance, *J. Chem. Phys.* **138**, 084304 (2013)
25. J.R. Gascooke, W.D. Lawrance, *J. Chem. Phys.* **138**, 134302 (2013)
26. E.A. Virgo, J.R. Gascooke, W.D. Lawrance, *J. Chem. Phys.* **140**, 154310 (2014)
27. J.R. Gascooke, E.A. Virgo, W.D. Lawrance, *J. Chem. Phys.* **142**, 024315 (2015)
28. J.R. Gascooke, E.A. Virgo, W.D. Lawrance, *J. Chem. Phys.* **143**, 044313 (2015)
29. D.L. Kokkin, T.C. Steimle, D. DeMille, *Phys. Rev. A* **90**, 062503 (2014)
30. N.J. Reilly, D.L. Kokkin, M. Nakajima, K. Nauta, S.H. Kable, T.W. Schmidt, *J. Am. Chem. Soc.* **130**, 3137 (2008)
31. N.J. Reilly, M. Nakajima, B.A. Gibson, T.W. Schmidt, S.H. Kable, *J. Chem. Phys.* **130**, 144313 (2009)
32. N.J. Reilly, M. Nakajima, T.P. Troy, N. Chalyavi, K.A. Duncan, K. Nauta, S.H. Kable, T.W. Schmidt, *J. Am. Chem. Soc.* **131**, 13423 (2009)
33. T.P. Troy, M. Nakajima, N. Chalyavi, K. Nauta, S.H. Kable, T.W. Schmidt, *J. Phys. Chem. A* **116**, 7906 (2012)
34. N.J. Reilly, M. Nakajima, T.P. Troy, D.L. Kokkin, N. Chalyavi, K. Duncan, K. Nauta, R.G. Sharp, T.W. Schmidt, S.H. Kable, *J. Phys: Conf. Ser.* **185**, 012037 (2009)
35. J.A. Joester, M. Nakajima, N.J. Reilly, D.L. Kokkin, K. Nauta, S.H. Kable, T.W. Schmidt, *J. Chem. Phys.* **127**, 214303 (2007)
36. M. Nakajima, J.A. Joester, N.I. Page, N.J. Reilly, G.B. Bacskay, T.W. Schmidt, S.H. Kable, *J. Chem. Phys.* **131**, 044301 (2009)
37. P.R. Stollenwer, B.C. Odom, D.L. Kokkin, T. Steimle, *J. Mol. Spectrosc.* **332**, 26 (2017)
38. D.L. Kokkin, T. Ma, T. Steimle, T.J. Sears, *J. Chem. Phys.* **144**, 244304 (2016)
39. W. Roth, P. Imhof, M. Gerhards, S. Schumm, K. Kleiner, *Chem. Phys.* **252**, 247 (2000)
40. D.H. Levy, *Science* **214**, 263 (1981)
41. D.R. Borst, D.W. Pratt, *J. Chem. Phys.* **113**, 3658 (2000)
42. G.H. Atkinson, C.S. Parmenter, *J. Mol. Spectrosc.* **73**, 52 (1978)
43. R.H. Page, Y.R. Shen, Y.T. Lee, *J. Chem. Phys.* **88**, 5362 (1988)
44. O.J. Maselli, J.R. Gascooke, W.D. Lawrance, M.A. Buntine, *J. Phys. Chem. C* **113**, 637 (2009)
45. O.J. Maselli, J.R. Gascooke, W.D. Lawrance, M.A. Buntine, *Chem. Phys. Lett.* **513**, 1 (2011)
46. A. Miani, E. Cane, P. Palmieri, A. Trombetti, *J. Chem. Phys.* **112**, 248 (2000)
47. O.J. Maselli, Ph.D. thesis, The University of Adelaide, 2010
48. M. Mons, J. Lecalve, F. Piuzzi, I. Dimicoli, *J. Chem. Phys.* **92**, 2155 (1990)
49. D.G. Lister, J.N. Macdonald, N.L. Owen, eds., *Internal rotation, inversion: an introduction to large amplitude motions in molecules* (Academic Press, London, 1978)
50. D.J. Nesbitt, M.A. Suhm, *Phys. Chem. Chem. Phys.* **12**, 8151 (2010)
51. E.B. Wilson, J.C. Decius, P.C. Cross, eds., *Molecular vibrations* (McGraw-Hill, London, 1955)
52. I. Kleiner, *J. Mol. Spectrosc.* **260**, 1 (2010)
53. P. Groner, *J. Mol. Spectrosc.* **278**, 52 (2012)
54. PROSPE: Programs for ROtational SPECTroscopy, <http://www.ifpan.edu.pl/~kisiel/prospe.htm>
55. V.V. Ilyushin, Z. Kisiel, L. Pszczólkowski, H. Mäder, J.T. Hougen, *J. Mol. Spectrosc.* **259**, 26 (2010)
56. E.B. Wilson Jr., C.C. Lin, D.R. Lide Jr., *J. Chem. Phys.* **23**, 136 (1955)
57. W. Gordy, R.L. Cook, *Microwave molecular spectra* (Wiley, New York, 1970), Chap. 12
58. K. Okuyama, N. Mikami, M. Ito, *J. Phys. Chem.* **89**, 5617 (1985)
59. K. Okuyama, N. Mikami, M. Ito, *Laser Chem.* **7**, 197 (1987)
60. T. Aota, T. Ebata, M. Ito, *J. Phys. Chem.* **93**, 3519 (1989)
61. H. Mizuno, K. Okuyama, T. Ebata, M. Ito, *J. Phys. Chem.* **91**, 5589 (1987)
62. G. Myszkiewicz, W.L. Meerts, C. Ratzer, M. Schmitt, *J. Chem. Phys.* **123**, 044304 (2005)
63. S. Tanaka, K. Okuyama, *J. Chem. Phys.* **134**, 084311 (2011)
64. J.G. Philis, V.S. Melissas, *J. Chem. Phys.* **127**, 204310 (2007)
65. J.A. Ruiz-Santoyo, J. Wilke, M. Wilke, J.T. Yi, D.W. Pratt, M. Schmitt, L. Álvarez-Valtierra, *J. Chem. Phys.* **144**, 044303 (2016)
66. M. Fujii, M. Yamauchi, K. Takazawa, M. Ito, *Spectrochim. Acta* **50A**, 1421 (1994)
67. J.M. Hollas, P.F. Taday, *J. Chem. Soc. Faraday Trans.* **87**, 3585 (1991)
68. P.J. Breen, E.R. Bernstein, H.V. Secor, J.I. Seeman, *J. Am. Chem. Soc.* **111**, 1958 (1989)
69. P.J. Morgan, L. Alvarez-Valtierra, D.W. Pratt, *Phys. Chem. Chem. Phys.* **12**, 8323 (2010)
70. R.A. Walker, E.C. Richard, K.-T. Lu, J.C. Weisshaar, *J. Phys. Chem.* **99**, 12422 (1995)
71. R.A. Walker, E.C. Richard, J.C. Weisshaar, *J. Phys. Chem.* **100**, 7333 (1996)
72. E.C. Richard, R.A. Walker, J.C. Weisshaar, *J. Chem. Phys.* **104**, 4451 (1996)
73. H. Kojima, K. Sakeda, T. Suzuki, T. Ichimura, *J. Phys. Chem. A* **102**, 8727 (1998)
74. P.J. Breen, J.A. Warren, E.R. Bernstein, J.I. Seeman, *J. Chem. Phys.* **87**, 1917 (1987)
75. L.H. Spangler, *Annu. Rev. Phys. Chem.* **48**, 481 (1997)
76. A.M. Gardner, A.M. Green, V.M. Tamé-Reyes, V.H.K. Wilton, T.G. Wright, *J. Chem. Phys.* **138**, 134303 (2013)
77. J.R. Gascooke, W.D. Lawrance, *J. Mol. Spectrosc.* **318**, 53 (2015)
78. J.H. Callomon, G.G. Chandler, *Appl. Opt.* **8**, 1133 (1969)
79. H.-L. Dai, R.W. Field, eds., in *Molecular dynamics and spectroscopy by stimulated emission pumping, Advanced series in physical chemistry* (World Scientific, New Jersey, 1995), Vol. 4
80. U. Boesl, H.J. Neusser, E.W. Schlag, *Z. Naturforsch. A* **33**, 1546 (1978)